



# Myosin Heavy Chain Converter Domain Mutations Drive Early-Stage Changes in Extracellular Matrix Dynamics in Hypertrophic Cardiomyopathy

Jeanne Hsieh<sup>1</sup>, Kelsie L. Becklin<sup>2</sup>, Sophie Givens<sup>1</sup>, Elizabeth R. Komosa<sup>1</sup>, Juan E. Abrahante Lloréns<sup>3</sup>, Forum Kamdar<sup>4</sup>, Brandon S. Moriarity<sup>2</sup>, Beau R. Webber<sup>2</sup>, Bhairab N. Singh<sup>1,2,5\*</sup> and Brenda M. Ogle<sup>1,2,5\*</sup>

<sup>1</sup>Department of Biomedical Engineering, University of Minnesota, Minneapolis, MN, United States, <sup>2</sup>Department of Pediatrics, University of Minnesota, Minneapolis, MN, United States, <sup>3</sup>University of Minnesota Informatics Institute (UMII), University of Minnesota, Minneapolis, MN, United States, <sup>4</sup>Department of Medicine, University of Minnesota, Minneapolis, MN, United States, <sup>5</sup>Stem Cell Institute, University of Minnesota, Minneapolis, MN, United States

## OPEN ACCESS

### Edited by:

Laura Iop,  
University of Padua, Italy

### Reviewed by:

Maksymilian Prondzynski,  
Boston Children's Hospital and  
Harvard Medical School, United States  
Kathleen Ruppel,  
Stanford University, United States

### \*Correspondence:

Bhairab N. Singh  
bnsingh@umn.edu  
Brenda M. Ogle  
ogle@umn.edu

### Specialty section:

This article was submitted to  
Stem Cell Research,  
a section of the journal  
Frontiers in Cell and Developmental  
Biology

Received: 12 March 2022

Accepted: 24 May 2022

Published: 16 June 2022

### Citation:

Hsieh J, Becklin KL, Givens S, Komosa ER, Lloréns JEA, Kamdar F, Moriarity BS, Webber BR, Singh BN and Ogle BM (2022) Myosin Heavy Chain Converter Domain Mutations Drive Early-Stage Changes in Extracellular Matrix Dynamics in Hypertrophic Cardiomyopathy. *Front. Cell Dev. Biol.* 10:894635. doi: 10.3389/fcell.2022.894635

More than 60% of hypertrophic cardiomyopathy (HCM)-causing mutations are found in the gene loci encoding cardiac myosin-associated proteins including myosin heavy chain (MHC) and myosin binding protein C (MyBP-C). Moreover, patients with more than one independent HCM mutation may be at increased risk for more severe disease expression and adverse outcomes. However detailed mechanistic understanding, especially at early stages of disease progression, is limited. To identify early-stage HCM triggers, we generated single (*MYH7* c.2167C > T [R723C] with a known pathogenic significance in the MHC converter domain) and double (*MYH7* c.2167C > T [R723C]; *MYH6* c.2173C > T [R725C] with unknown significance) myosin gene mutations in human induced pluripotent stem cells (hiPSCs) using a base-editing strategy. Cardiomyocytes (CMs) derived from hiPSCs with either single or double mutation exhibited phenotypic characteristics consistent with later-stage HCM including hypertrophy, multinucleation, altered calcium handling, metabolism, and arrhythmia. We then probed mutant CMs at time points prior to the detection of known HCM characteristics. We found *MYH7/MYH6* dual mutation dysregulated extracellular matrix (ECM) remodeling, altered integrin expression, and interrupted cell-ECM adhesion by limiting the formation of focal adhesions. These results point to a new phenotypic feature of early-stage HCM and reveal novel therapeutic avenues aimed to delay or prohibit disease onset.

**Keywords:** hypertrophic cardiomyopathy, gene editing, MYH7, MYH6, extracellular matrix, integrins

## 1 INTRODUCTION

Hypertrophic cardiomyopathy (HCM) is the most common gene-linked cause of cardiac disease, affecting nearly 0.2% of the population globally (Semsarian et al., 2015). Clinical manifestations of HCM are highly variable, ranging from mild arrhythmias to sudden cardiac death (SCD), possibly due to single or multiple defects that give rise to myocyte disarray, fibrosis, hypertrophy, and heart

failure (Marian and Braunwald, 2017). Among the many sarcomeric gene mutations associated with HCM, cardiac  $\beta$ -myosin heavy chain ( $\beta$ -MHC), myosin-binding protein C (MyBP-C), and cardiac Troponin T (cTnT) are the most prevalent (Burke et al., 2016; Marian and Braunwald, 2017). Some mutations result in early disease phenotypes, whereas others lead to late progressive HCM (Sedaghat-Hamedani et al., 2018). Whether variability in disease state is due to distinct molecular defects is largely unknown. While mutation type cannot currently be used to predict disease outcomes and guide management, patients with multiple independent sarcomere mutations have been identified to have more severe pathology including a higher prevalence of heart failure and SCD (Kelly and Semsarian, 2009; Girolami et al., 2010; Maron et al., 2012; Weissler-Snir et al., 2017). These findings highlight the need for comprehensive analysis using one or more HCM mutations. Here we focus our efforts on dual mutations in *MYH7* and *MYH6*.

*MYH7* encodes  $\beta$ -MHC and is composed of a N-terminal globular head domain and C-terminal coiled-coil ends with light meromyosin (LMM) domain (Homburger et al., 2016). The binding of  $\text{Ca}^{2+}$  exposes the myosin-binding sites on the actin filaments, leading to the formation of actin-myosin junctions and associated ability to glide along the actin base (Homburger et al., 2016). In the presence of ATP, these complexes are detached, and the ATPase activity of the head domain hydrolyzes ATP to initiate the next cycle of contraction (Homburger et al., 2016). A direct correlation between *MYH7* mutations, ATP utilization, and oxygen consumption has been established, however, whether these defects are associated only with the mutation that affects the active sites of the head-domain or altered mechanical properties of converter-domain or both is not completely defined (Becker et al., 1997; Mosqueira et al., 2018). Although several HCM mutations are in the *MYH7* locus, significant clusters are found in the converter domain, also known as a “hot spot” of mutation (Homburger et al., 2016). Biophysical studies have shown that mutations in the converter region alter fiber stiffness, gliding velocity, and cross-bridge elasticity (Kohler et al., 2002; Kawana et al., 2017), and could also affect the super relaxed state (Toepfer et al., 2020; Vander Roest et al., 2021), thereby impacting the motor function of the myosin proteins; however, the functional impact of these mutations remains unclear.

*MYH6* gene encodes the other major MHC isoform,  $\alpha$ -MHC. *MYH6* is the predominant ventricular form in small mammals such as mice and rat. Additionally, it is expressed primarily in the atria in mature mammalian hearts and in the ventricle at embryonic stages and shares nearly 93% sequence homology with *MYH7* (McNally et al., 1989). Despite sequence and structural similarities between the  $\alpha$ -MHC and  $\beta$ -MHC isoforms,  $\alpha$ -MHC shows 150%–300% higher contractile velocity and ~70% higher affinity for the actin filaments than  $\beta$ -MHC proteins (Alpert et al., 2002; Locher et al., 2009). Like *MYH7* gene mutations, a number of HCM-causing mutations have been documented in the *MYH6* locus. For example, R795Q results in late onset HCM (Niimura et al., 2002), and R721W showed 50% increased lifetime risk for sick sinus syndrome in

carriers of this variant (Holm et al., 2011). Similar to *MYH7*, a mutation in the converter domain of *MYH6* is associated with congenital heart defects (Bjornsson et al., 2018). To our knowledge, phenotypic as well as mechanistic studies from such clinically-relevant *MYH6* mutations have not yet been performed.

hiPSC-derived cardiomyocytes (hiPSC-CMs) provide a pathophysiologically relevant approach to investigate *human* HCM and to design novel therapeutics (Lan et al., 2013; Mosqueira et al., 2018). Gene editing approaches further augment the utility of hiPSC-CMs to determine how certain mutations manifest the clinical disease phenotype. This approach also allows for studies of the mutation with an isogenic control to manage the genetic variability of individuals that may influence disease conditions (Bhagwan et al., 2020). Several studies have utilized gene-edited hiPSC-CMs to investigate the molecular details of HCM (Lan et al., 2013; Mosqueira et al., 2018; Yang et al., 2018). This approach is particularly valuable as available human tissue is largely limited to late-stage biopsy or cadaveric tissue. In addition, rodent models are of limited value for the current study since mice predominantly express *MYH6* in the heart as compared to *MYH7* in the human heart with significantly different cardiac electrophysiological properties relative to humans (Lowey et al., 2008). Recently, Mosqueira et al. demonstrated an HCM phenotype in *MYH7* R453C mutant hiPSC-CMs with sarcomeric disarray and arrhythmia (Mosqueira et al., 2018). Similarly, studies using *MYH7* E848G mutant hiPSC-CM showed disrupted interactions between  $\beta$ -MHC and MyBP-C with reduced contractility (Yang et al., 2018). These studies support the benefits of hiPSC-CMs to study HCM.

Here, we used hiPSC-CMs to evaluate the impact of converter domain mutations in the *MYH7* and *MYH6* locus on the pathogenicity of HCM and identified early ECM changes that precede later-stage physiologic defects associated with HCM. These studies are the first to link ECM dynamics with HCM onset and therefore provide a new avenue for drug discovery aimed at prevention or delay of disease symptoms.

## 2 MATERIALS AND METHODS

### 2.1 Gene Editing hiPSC Lines

#### 2.1.1 Guide RNA Design and Genomic DNA Analysis

The major isoform of *MYH7* for single-guide RNA (sgRNA) design was identified using NCBI (<https://www.ncbi.nlm.nih.gov/>) and the guide (gtatcgatcctgaaccag) was chosen based on the on location of a PAM site placing the target C within the five base pair editing window (Komor et al., 2016). The first passage after electroporation genomic DNA was isolated using QuickExtract™ (Lucigen), following manufacturer protocol. The target genomic locus was subsequently PCR amplified using AccuPrime Taq Hifi (ThermoFisher) (*MYH7* forward primer: cagtgcacaagccaggatca, reverse primer: ttggtgtggcacaactgta; *MYH6* forward primer: gtgccccagagctcatagaa, reverse primer: ggcttctgctcctaaactc) followed by Sanger sequencing of the PCR amplicon (ACGT). Sanger sequencing traces of base-edited samples were analyzed using EditR ([z.umn.edu/editr](http://z.umn.edu/editr)) (Kluesner et al., 2018). After clones were

selected the top two off-target sites were sequenced following the same protocol as clonal selection (CPQ forward primer: agggaa ccatggccataaatgt, reverse primer: gcctccctggggaagtata; MYO5b forward primer: gccgagcctcagaagtgtag, reverse primer: cccctccc agtagaactca).

### 2.1.2 hiPSC Electroporation and Clonal Isolation

The control hiPSC line was kindly provided by Dr. Jianyi Zhang (University of Alabama at Birmingham), this hiPSC line was reprogrammed from cardiac fibroblasts of a healthy female donor and modified to overexpress cyclin D2 to enhance the yield of cardiac differentiation (Zhu et al., 2018; Zhao et al., 2021). To generate mutant hiPSCs, 2 h prior to electroporation, hiPSCs were treated with 10  $\mu$ M ROCK inhibitor (Y27632 dihydrochloride, Tocris). Cells were then passaged and 250 K cells were then spun down in PBS. Cells were resuspended in P3 Primary Cell Nucleofector™ Solution containing Supplement 1 (Lonza, Switzerland) and 1  $\mu$ g of chemically modified sgRNA (Synthego, Menlo Park, CA) and 1.5  $\mu$ g codon optimized BE4 mRNA (TriLink Biotechnologies, San Diego, CA) and placed in the 20  $\mu$ L cuvette provided and CB-150 was the Amaxa protocol used. Cells were given 10  $\mu$ M ROCKi for 48 h post electroporation followed by normal culturing conditions. For hiPSC single cell isolation ~300 single cell suspended iPSC were cultured in a 10 cm dish with 10  $\mu$ M ROCKi for 48 h. For the next 10 days cells were given daily media changes and then colonies were isolated using a 10  $\mu$ L pipette to scrape half of the colony for isolated culture and half the colony for genomic DNA isolation.

## 2.2 Cardiac Differentiation

Isogenic control hiPSC-CMs and mutant hiPSC-CMs were obtained *via* the fully defined direct cardiac differentiation by modulating Wnt/b-catenin signaling. Briefly, hiPSCs were cultured on Matrigel-coated 6-well plates in mTeSR1 medium for 5 days to reach 80%–90% confluency. All hiPSC lines used for differentiation were between passage 57–78. To harvest singularized cells, the culture medium was removed, and the wells were washed one time with sterile DPBS, then added 1 ml of room-temperature Accutase into each well. The plates were transferred into the incubator to allow Accutase to react at 37°C for 8 min. 0.5 ml of mTeSR1 medium was added into each well to stop Accutase reactions. The singularized cells were resuspended in mTeSR1 with 5  $\mu$ M ROCK inhibitor (Y27632), seeded with the density of  $5 \times 10^5$  cells/well on Matrigel-coated 24-well plates and maintained at 37°C, 5% CO<sub>2</sub> incubator for 24 h. After 24 h, on Day -1, 1 ml of fresh mTeSR1 medium was added to each well. On Day 0, initiation of cardiac differentiation was performed on 100% confluent hiPSCs. At that time, 1 ml of RPMI/B-27 without insulin (RPMI minus) medium with 8  $\mu$ M GSK3- $\beta$  inhibitor (CHIR99021) was added into each well for 24 h in the 37°C, 5% CO<sub>2</sub> incubator to induce mesoderm. On Day 1, CHIR99021 medium was replaced with fresh RPMI/B27 minus medium. On Day 3, 0.5 ml of exhausted medium from each well was collected and mixed 1:1 with fresh RPMI/B27 minus insulin medium. Wnt inhibitor (IWP2) was added into the mixed medium to achieve the concentration of

5  $\mu$ M. Each well was incubated with IWP2 for 48 h to induce cardiac differentiation. On Day 5, fresh RPMI/B27 minus insulin was added into each well. On Day 7 and every 3 days thereafter, fresh maintenance medium, RPMI/B-27 medium, was added to each well. Spontaneous twitching was observed on Day 8, and robust spontaneous contraction occurred by Day 12. To purify the cardiomyocyte population, lactate enrichment was performed on Day 15–18 *via* adding 1 ml/well of DMEM (without glucose) with 4 mM sodium L-lactate every 2 days. On Day 19 and every 3 days thereafter, cells were maintained in RPMI/B27 medium.

## 2.3 Immunohistochemical Staining

Cultured hiPSC-CMs were fixed with 4% paraformaldehyde (PFA) for 15 min and then washed and stored in PBS at 4°C. To perform immunostaining, cultured hiPSC-CMs were permeabilized by 0.2% Triton X-100 at room temperature for 1 h, washed with PBS 3 times, and then added blocking buffer (2.5 g non-fat dry milk in 50 ml of 0.2% Triton X-100) to incubate at room temperature for 2 h. Washed with PBS 3 times before adding primary antibody (mouse anti-cTnT, 1:200 dilution in BGST buffer) for overnight incubation at 4°C. Washed with 0.2% Tween 20 for 2 times and PBS for 2 times before adding secondary antibody (Alexa Fluor 647 goat anti-mouse IgG, 1:500 dilution in BGST buffer), plates were covered by aluminum foil and incubated at room temperature for 1.5 h. Washed with 0.2% Tween 20 for 2 times and PBS for 2 times before staining for nuclei with 0.1  $\mu$ g/ml of DAPI dye for 15 min at room temperature. Washed with PBS 3 times to remove the excess dye and stored in PBS at 4°C before imaging. For co-staining of pFAK and cTnT, we followed the protocol above with slight modifications. Briefly, after fixation, we permeabilized the cardiomyocytes using 0.2% Triton X-100 in PBS (0.2% PBST) for 10 min followed by washing with 0.1% PBST three times. The cells were blocked using 5% BSA/0.1% PBST for 1 h and incubated with primary antibodies, cTnT-1:300; pFAK-1:1,000 in the blocking solution in a humidified chamber overnight. Subsequently, the cells were washed 4 times with 0.1% PBST followed by incubation with secondary antibodies (1:500) for 1 h at room temperature. Cells were washed 4 times and stained for nuclei using DAPI (1:1,000), and images using Leica fluorescence microscope.

## 2.4 ADP/ATP Assay

ADP/ATP assay was performed as per manufacturer's instructions using ADP/ATP Ratio Assay Kit (Bioluminescent) (Abcam, ab65313). Isogenic control and mutant hiPSCs were differentiated to cardiomyocytes as described above and single-cell suspension was obtained at each time point. A total of 50,000 cells from each condition for each time point were re-suspended in the 250  $\mu$ L of nucleotide releasing buffer for 5 min at room temperature. A total of 50  $\mu$ L of the cell lysate was added to the reaction mix and incubated for 2 min before measuring the ATP levels. To measure the ADP levels, 10  $\mu$ L of ADP converting enzyme was added to the reaction mix and fluorescence was measured after 2 min of incubation using the bioluminescence plate reader.

## 2.5 RNA Isolation and qPCR Analysis

Total RNA was isolated from undifferentiated and differentiated isogenic control and R723C hiPSCs using the RNeasy kit (Qiagen) according to the manufacturer's protocol. Briefly, washed the cells once with sterile PBS and lysed in RLT-lysis buffer for specific time points. RNA isolation was performed as per the protocol, followed by on-column DNA digestion to remove any traces of DNA as per the instructions. For cDNA synthesis, 100–1000 ng of total RNA was used and synthesized using the SuperScript IV VILO kit (Thermo Fisher Scientific) according to the manufacturer's protocol. Quantitative PCR (qPCR) was performed using gene-specific oligos and the SYBR-green method. The list of oligos used is provided in **Supplementary Table S3**.

## 2.6 Bulk-RNA Sequencing and Analysis

The total RNA was isolated as described above. For the bulk-RNaseq analysis, 1 µg of total RNA was submitted to Novogene (<https://en.novogene.com/>) for sequencing and data analysis. Downstream analysis was performed using a combination of programs including STAR, HTseq, Cufflink, and our wrapped scripts. Alignments were parsed using Tophat program and differential expressions were determined in R using the package DESeq2/edgeR. GO and KEGG enrichment was implemented by the ClusterProfiler. Gene fusion and difference of alternative splicing events were detected by Star-fusion and rMATS software. Reference genome and gene model annotation files were downloaded from the genome website browser (NCBI/UCSC/Ensembl) directly. Indexes of the reference genome were built using STAR and paired-end clean reads were aligned to the reference genome using STAR (v2.5). STAR used the method of Maximal Mappable Prefix (MMP) which can generate a precise mapping result for junction reads. HTSeq v0.6.1 was used to count the read numbers mapped of each gene. And then FPKM of each gene was calculated based on the length of the gene and the reads count mapped to this gene. FPKM, Reads Per Kilobase of exon model per Million mapped. reads, considers the effect of sequencing depth and gene length for the reads count at the same time, and is currently the most used method for estimating gene expression levels. Differential expression analysis between two conditions/groups (two biological replicates per condition) was performed using the DESeq2 R package (2\_1.6.3). DESeq2 provides statistical routines for determining differential expression in digital gene expression data using a model based on the negative binomial distribution. The resulting *p*-values were adjusted using the Benjamini and Hochberg's approach for controlling the False Discovery Rate (FDR). Genes with an adjusted *p*-value <0.05 found by DESeq2 were assigned as differentially expressed. To identify the correlation between differences, we clustered different samples using expression level FPKM to see the correlation using the hierarchical clustering distance method with the function of the heatmap, SOM (Selforganization mapping), and kmeans using silhouette coefficient to adapt the optimal classification with default parameter in R.

## 2.7 Statistical Analysis

All experiments were repeated at least two times and the values presented are mean ± standard error of the mean (SEM) from the replicates of at least two independent experiments. Statistical significance was determined using the Student *t* test when comparing two groups and ONE-WAY ANOVA with multiple comparisons when comparing more than two groups. A *p*-value < 0.05 was considered a significant change and was highlighted in each panel by an asterisk.

## 3 RESULTS

### 3.1 MYH7 R723C Mutation can Result in an Early Pathogenic HCM Phenotype

Mutations in the *MYH7* locus result in severe HCM phenotypes in human patients (Burke et al., 2016) especially those in the converter domain, a “hot spot” for HCM mutations (**Supplementary Table S1**). Through database searches, we identified a subset of converter domain mutations that contain a total of 14 patients with a single mutation of *MYH7* R723C (**Supplementary Table S2**). There was gene penetration in 64% (9/14) patients. The mean age of the gene penetrant patients was 29 ± 13 years and maximal wall thickness was 24 ± 10 mm (range 11–38 mm). Three patients were described to have symptoms which included heart failure. Patient 1 was symptomatic at age 12 and underwent cardiac transplant at the age of 16. Patient 1's father was the proband and had the same mutation and end-stage heart failure, but further clinical information was not available to include him in the study. Tesson et al. described an Italian family with 11 members with a *MYH7* R723C mutation in which the proband was incidentally identified on routine screening. In this family, patients 8 and 9 were monozygotic twins and gene penetrance was undetermined for patient 9 given ECG changes but normal indexed wall thickness. Above clinical observations indicate the *MYH7* R723C mutation can result in early pathologic HCM to asymptomatic incomplete penetrance. Additional clinical data on this mutation coupled with *in vitro* mechanistic studies will be important to understand gene penetrance, symptoms, and survival. Further, no study has explored the possible compensatory impact of wild-type α-MHC protein in these patients given the structural similarity of β-MHC to α-MHC. In the current study, we investigate the mechanisms that govern initial onset of HCM in the presence of pathogenic *MYH7* mutation and another mutation in the corresponding position of the *MYH6* locus with unknown clinical significance.

### 3.2 Generation and Characterization of Isogenic Control and MHC Mutant hiPSC Lines

Multiple reports have shown the pathological symptoms of c.2167C > G (R723G) and c.2167C > T (R723C) mutations in *MYH7* gene locus leading to hypertrophic cardiomyopathy in human patients (Homburger et al., 2016; Kraft et al., 2016). Interestingly, while the R723G mutation is well-described

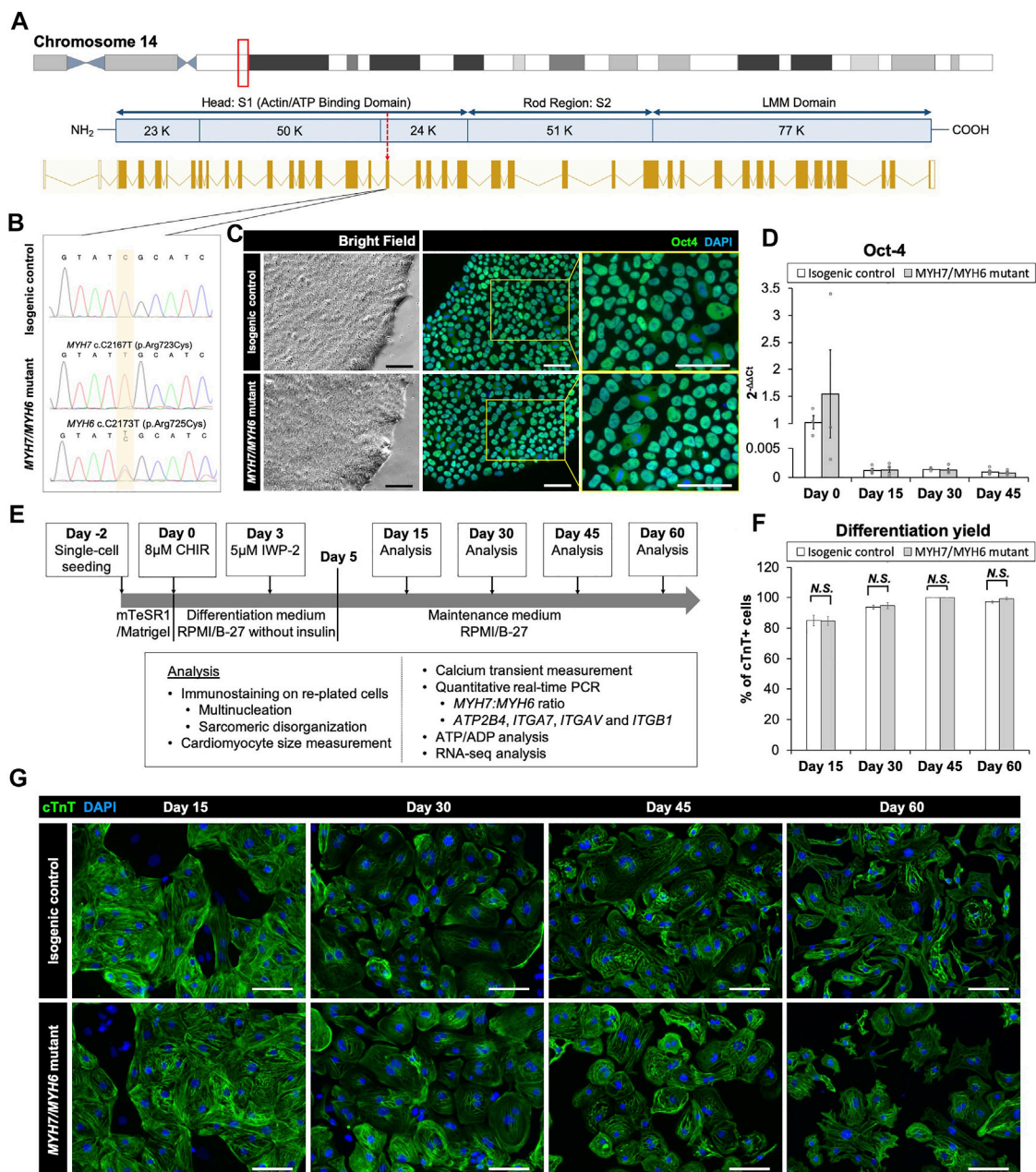


**FIGURE 1** | Base editing and characterization of the MYH7/MYH6 mutant hiPSCs. **(A)** Schematic of MYH7 locus as shown in the red box on chromosome 14 and c.2167 location as pointed by the red arrow for base editing. **(B)** Chromatogram of MYH7 mutant locus in hiPSCs showing c.C2167T (p.Arg723Cys, p.R723C) mutation and its isogenic parental genotype. **(C)** Bright field images and immunostaining of Oct-4 using the isogenic control and MYH7/MYH6 mutant hiPSCs. DAPI labels the nuclei (blue). **(D)** qPCR analysis for Oct-4 expression level using RNA isolated from the isogenic control and MYH7/MYH6 mutant hiPSCs. **(E)** Cardiac differentiation timeline and analysis regime. **(F)** Quantitative analysis of the differentiation efficiency based on the cTnT staining in the control and MYH7/MYH6 mutant cardiomyocytes. Note that mutation did not result in any significant difference in the cardiomyocyte differentiation efficiency. **(G)** Cardiac Troponin T (cTnT) and DAPI-stained hiPSC-CMs on Day 15, 30, 45, and 60 after the start of differentiation. Data represents mean  $\pm$  SEM. (Scale Bar = 100  $\mu$ m) (N.S.: not significant; Student *t* test).

using biochemical, structural, and gene-editing approaches (Homburger et al., 2016; Kraft et al., 2016; Kawana et al., 2017), the impact of R723C mutation remains unclear, and the functional and mechanistic details are not yet defined. The arginine residue at the 723 location is highly conserved across multiple species (**Supplementary Figures S1A,B**) and mutation

in this region has been shown to alter mRNA secondary structure of MYH7 (Rose et al., 2020). To investigate the earlier stage MHC mutation-associated HCM pathology and to account for the effect of wild-type  $\alpha$ -MHC expressed by immature human induced pluripotent stem cell-derived cardiomyocytes (hiPSC-CMs) in 2D culture system, we utilized CRISPR/Cas9 base editing to

generate a homozygous *c.2167C > T* mutation in the *MYH7* locus (**Figure 1A**; **Supplementary Figures S2A–C**) with an analogous heterozygous *c.2173C > T* mutation in the *MYH6* locus in a hiPSC line reprogrammed from cardiac fibroblasts of a healthy female donor and modified to overexpress cyclin D2 to enhance differentiation yield (Gaudelli et al., 2017; Zhu et al., 2018; Webber et al., 2019; Zhao et al., 2021). We identified and expanded a clonal population of mutated cells with the targeted gene mutations of cytosine (C) to thymidine (T) at *c.2167C > T* and *c.2173C > T* positions. Sequencing showed a single chromatogram peak at the targeted positions, with no off-target effect (**Figure 1B**). Initially, we evaluated the pluripotency of the gene-edited lines using the *MYH7* R723C and *MYH6* R725C (*MYH7/MYH6*) dual mutant hiPSCs and the corresponding isogenic control hiPSCs. Immunostaining using *OCT4* antibody showed no difference between control and mutant lines (**Figure 1C**). Further, qPCR analysis demonstrated similar expression of *OCT4* transcripts in the control and mutant lines (**Figure 1D**). These results indicate that the stemness of mutant hiPSCs was not affected by the mutation or base editing procedure.

To assess the cardiomyocyte differentiation potential of the *MYH7/MYH6* mutant, single *MYH7* R723C (*MYH7*) mutant and the isogenic control lines, we differentiated the lines using a small-molecule protocol (Lian et al., 2012) and performed an array of analyses as schematized in **Figure 1E**. Spontaneous beating was observed between Day 8 and Day 12 of differentiation in both control and mutant lines. As expected, the *OCT4* transcripts were greatly reduced at Day 15 relative to Day 0 and remained low throughout the differentiation (**Figure 1D**, Day 15–45). Next, we assessed the efficiency of cardiomyocyte differentiation using immunofluorescence staining for cardiac troponin T (cTnT) up to Day 60 of differentiation (**Figures 1F,G**). Quantification of cTnT+ cells relative to DAPI-labeled nuclei revealed no significant difference in the differentiation efficiency between control and *MYH7/MYH6* mutant hiPSC-CMs (**Figure 1F**). As indicated by the percentage of cTnT+ cells, both mutant and the control lines exhibited more than 85% differentiation efficiency before lactate purification (Day 15) and more than 99% differentiation efficiency after lactate purification (Day 30, 45, and 60). There was no difference on the percentage of cTnT+ cells among the hiPSC-CMs of the *MYH7* mutant, *MYH7/MYH6* mutants, and the isogenic controls (**Supplementary Figure S3A**). These results indicate that the *MYH7* and *MYH7/MYH6* mutations did not affect cardiomyocyte differentiation potential.

### 3.3 *MYH7/MYH6* and *MYH7* Mutant hiPSC-CMs Recapitulate HCM Cellular Phenotypes

Several studies have utilized patient-derived or gene-edited hiPSC-CMs to model HCM phenotypes *in vitro* with supportive as well as variable findings (Lan et al., 2013; Kraft et al., 2016; Yang et al., 2018; Bhagwan et al., 2020). These differences may be dependent upon the type of mutation

and location (Bhagwan et al., 2020). To evaluate the impact of *MYH7/MYH6* and *MYH7* mutations on HCM phenotypes, we carried out a series of studies comparing the mutant hiPSC-CMs to the corresponding isogenic control hiPSC-CMs. Initially, we undertook analyses of cellular-scale features over time. To evaluate cellular hypertrophy, we analyzed the singularized cells prior to attachment to well plates and found that both *MYH7/MYH6* mutant cells and *MYH7* mutant cells were significantly larger in size than the isogenic control cells (**Supplementary Figures S3B,C**). We next counted the number of nuclei per cell and found a significant increase in multinucleated cells in the mutant hiPSC-CMs (**Supplementary Figure S3D**). At Day 15 of differentiation, mutant hiPSC-CMs had slightly lower number of multinucleated cells than the isogenic control hiPSC-CMs, while at Day 45 of differentiation, both *MYH7/MYH6* and *MYH7* mutant hiPSC-CMs had statistically significant higher number of multinucleated cells than the isogenic lines.

With little difference in cellular scale features among the two *MYH7/MYH6* mutant lines and one *MYH7* mutant line, we focused remaining comparisons on one isogenic control line and one *MYH7/MYH6* mutant line for a more detailed study of HCM phenotype progression over four different time points (i.e., Day 15, 30, 45, and 60 of differentiation). In this way we accounted for possible functional compensation of *MYH6* expressed at early developmental time points and correspondingly muted HCM phenotype in the *MYH7* single mutant. We found that while both control and *MYH7/MYH6* mutant hiPSC-CMs increased cardiomyocyte size over time, *MYH7/MYH6* mutant hiPSC-CMs were significantly larger than the control hiPSC-CMs at all time points (**Figures 2A,B**). This hypertrophic phenotype was further verified using FACS analysis of the singularized cardiomyocytes from control and *MYH7/MYH6* mutant lines between Day 15–45 (**Supplementary Figures S4A,B**). Interestingly, we observed a gradual decline in the overall cell density in the mutant lines relative to the control lines after the lactate purification (**Supplementary Figures S5B,C**). Further, the adherent cell area of the re-plated hiPSC-CMs showed no significant difference between the mutant and control lines at any of the four time points (**Supplementary Figure S5D**). Given the fact that cell volume is increased in the mutant, these data suggest cell spreading is also compromised in the mutant. Regarding multinucleation, quantitative analysis revealed that *MYH7/MYH6* mutant hiPSC-CMs had significantly more multinucleated cells than the control hiPSC-CMs from Day 30 of differentiation, and the difference was most pronounced at Day 45 with a two-fold increase in the *MYH7/MYH6* mutant condition ( $27\% \pm 5\%$ ) relative to control ( $12\% \pm 3\%$ ) (**Figures 2D,E**).

We then assessed the ratio of *MYH7:MYH6* transcripts using qPCR and found an increase in the mutant cardiomyocytes relative to the control isogenic lines (**Figure 2C**). A similar increase in the *MYH7:MYH6* ratio has been documented in hypertrophic patients (Lowe et al., 1997; Mosqueira et al., 2018). Further, our analysis revealed that the increase in *MYH7:MYH6* ratio was mainly caused by a

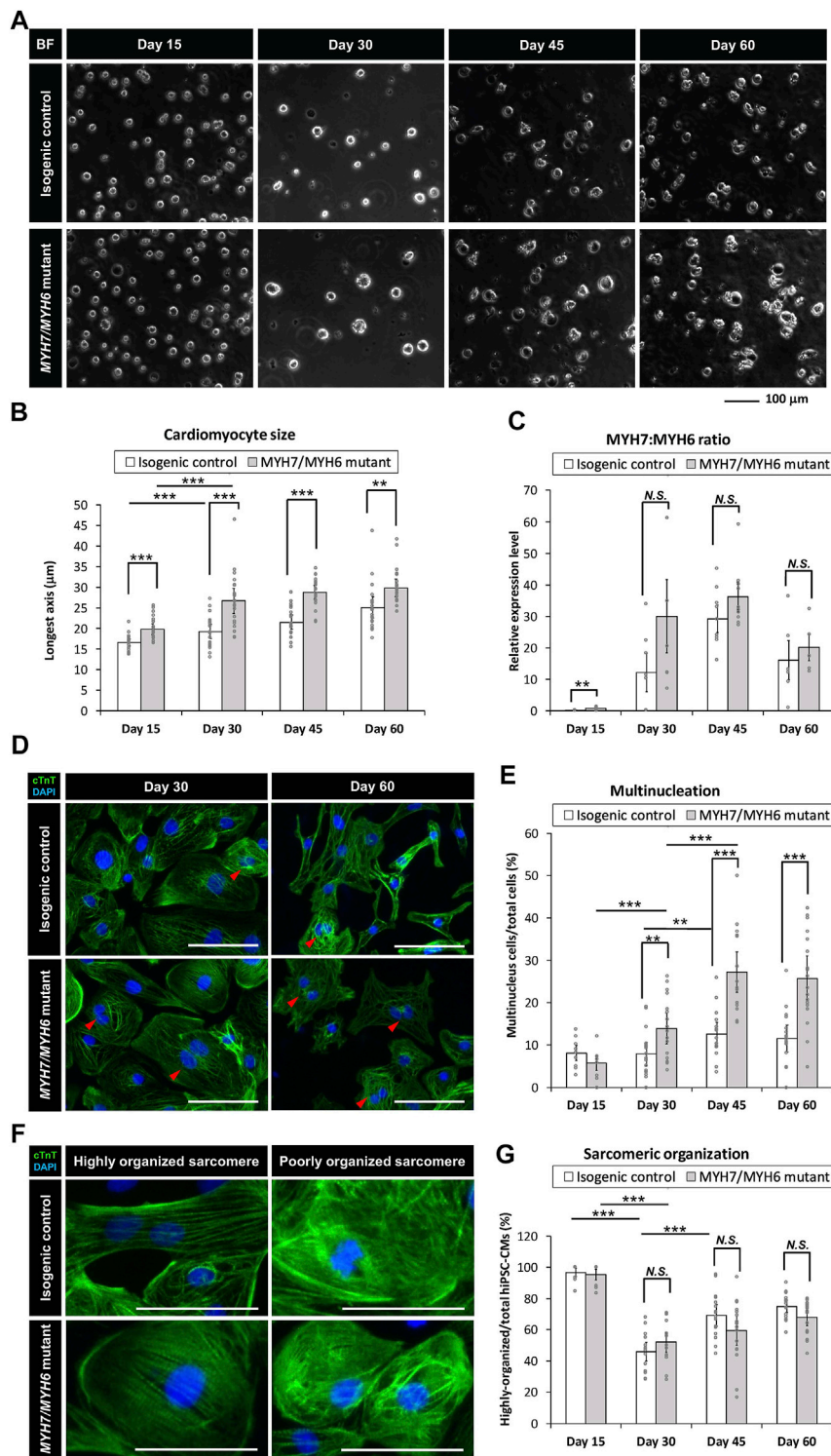
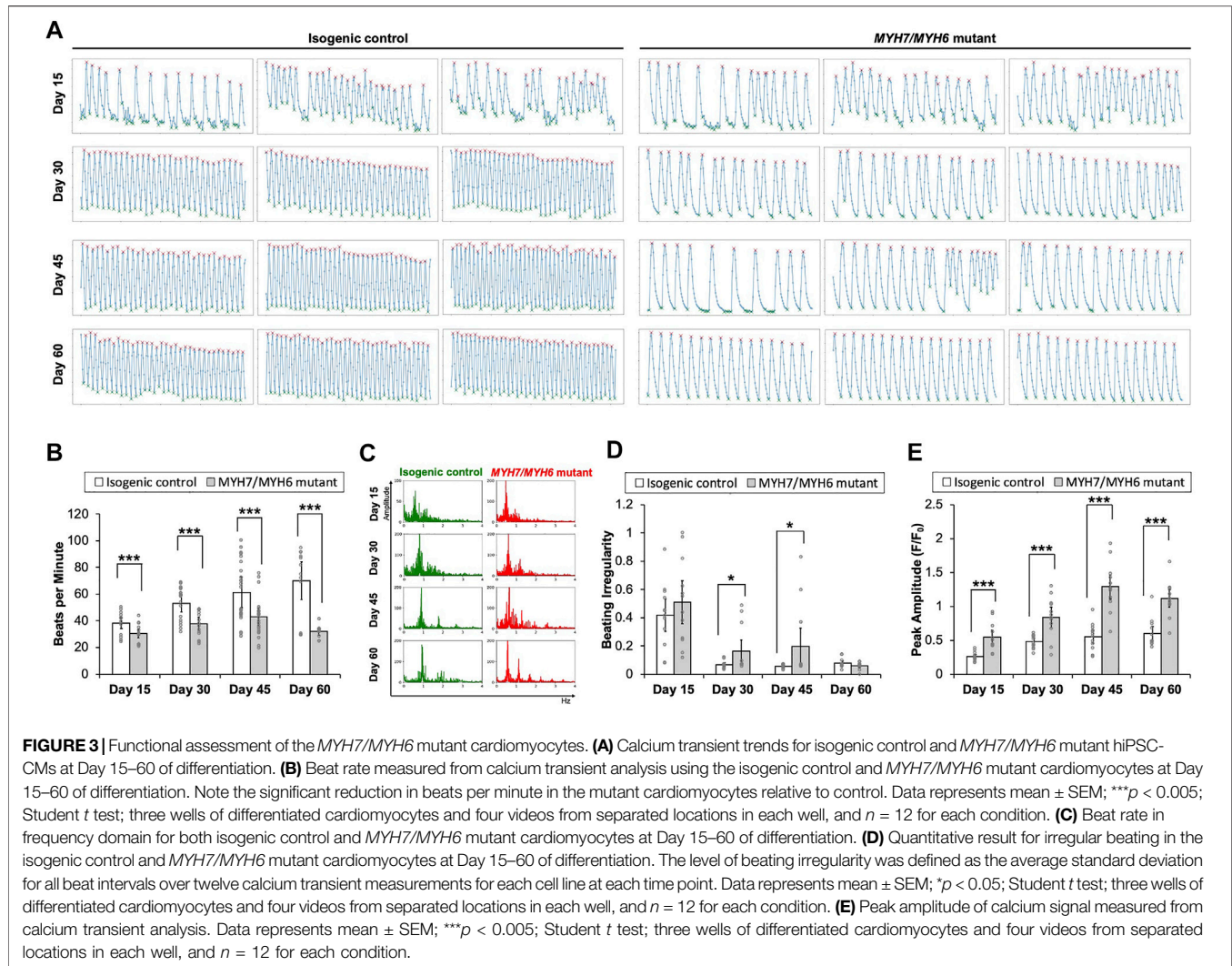


**FIGURE 2** | *MYH7/MYH6* mutation recapitulates the hypertrophic cardiomyopathy phenotype in the hiPSC-CMs. **(A,B)** Bright-field images **(A)** and quantification (longest axis) **(B)** of the re-plated control and mutant cardiomyocytes prior to their attachment to the substrate to analyze their size at Day 15–60 of differentiation. Notice the hypertrophy of the mutant cells from Day 15–60. (Scale Bar = 100  $\mu$ m). Data represents mean  $\pm$  SEM. (\*\* $p < 0.01$ ; \*\*\* $p < 0.005$ ; Student *t* test;  $n = 24$  for six randomly picked particles with round and intact boundary from four bright field images per condition) **(C)** *MYH7:MYH6* ratio obtained from qPCR analysis. Data represents mean  $\pm$  SEM. (\*\* $p < 0.01$ ; *N.S.*: not significant; Student *t* test; three wells for each condition and two experimental replicates for Day 15, Day 30, and Day 60, three experimental replicates for Day 45;  $n = 6$  for Day 15, Day 30, and Day 60, respectively, and  $n = 9$  for Day 45 conditions) **(D)** Representative images of cTnT-

(Continued)

**FIGURE 2** | Immunostained and DAPI-stained hiPSC-CMs to visualize nucleation in the differentiated cardiomyocytes using the isogenic control and *MYH7/MYH6* mutant lines. Red arrows indicate multi-nucleated cells. Left images show Day 30 re-plated hiPSC-CMs and Right images show Day 60 re-plated hiPSC-CMs. (Scale Bar = 100  $\mu$ m). **(E)** Bar graph shows that quantification of the percentage of hiPSC-CMs with more than one nucleus. Note significant increase in the multinucleated cells in the mutant conditions relative to control cells. Data represents mean  $\pm$  SEM. (\*\* $p < 0.01$ ; \*\*\* $p < 0.005$ ; Student *t* test;  $n = 9$  immunostained images for Day 15 conditions,  $n = 18$  immunostained images for Day 30, Day 45, and Day 60, respectively). **(F)** High magnification fluorescence images of cTnT and DAPI-stained hiPSC-CMs to analyze the sarcomeric organization in the control and R723C mutant cardiomyocytes. (Scale Bar = 50  $\mu$ m). **(G)** Bar graph shows percentage of hiPSC-CMs with highly organized sarcomere. Data represents mean  $\pm$  SEM. (\*\*\* $p < 0.005$ ; N.S.: not significant; Student *t* test;  $n = 9$  immunostained images for Day 15 conditions,  $n = 18$  immunostained images for Day 30, Day 45, and Day 60, respectively).



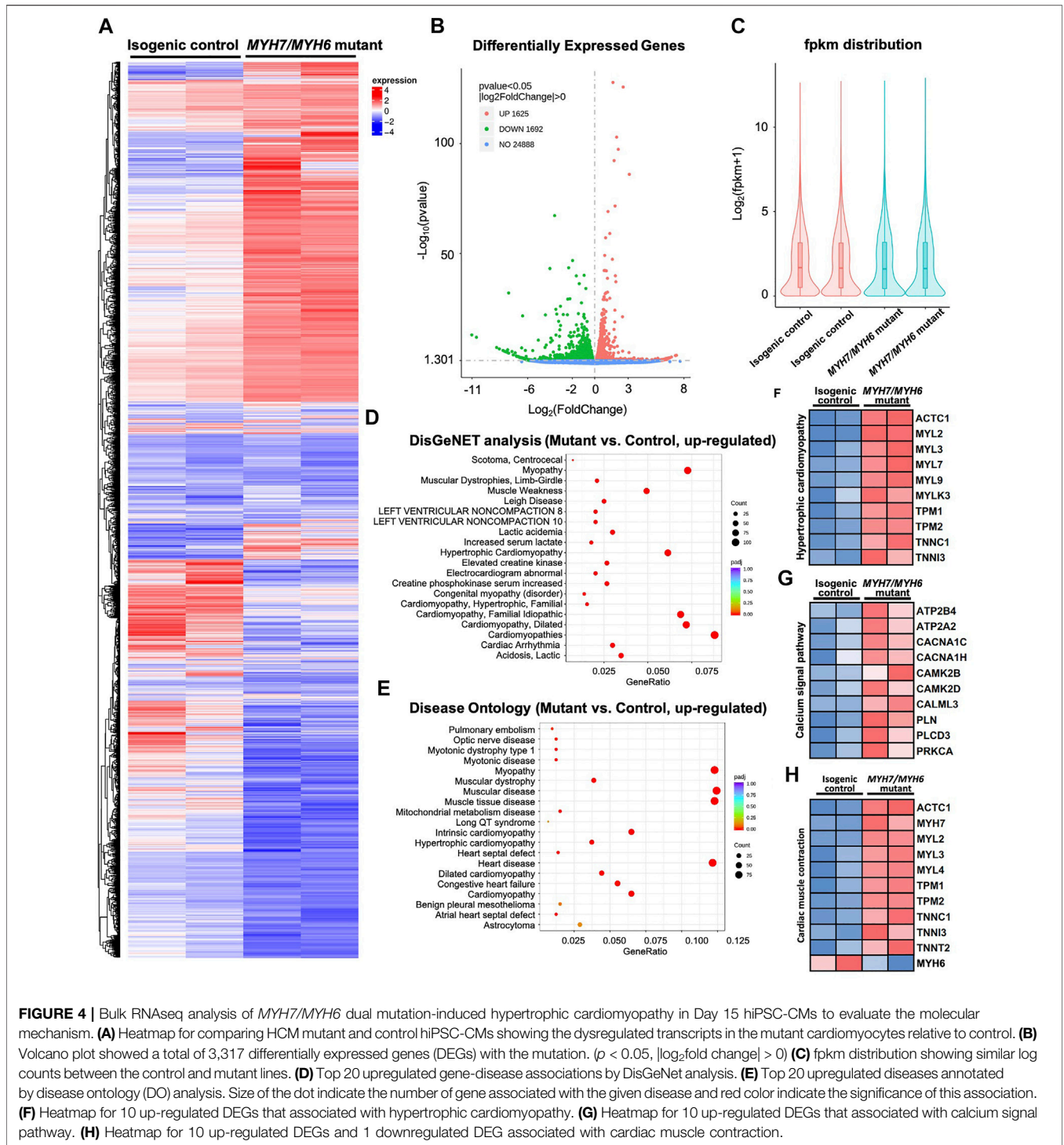
reduced level of expression of *MYH6* (less energy efficient) relative to the control, without much change in *MYH7* (more energy efficient) transcripts. Another HCM phenotype reported with *MYH7* mutations is sarcomere disorganization and myofibrillar disarray; however, we did not find any difference in the percentage of cells with irregular and unorganized sarcomeric structures in the hiPSC-CMs from control and mutant cells at any of the time points examined (Figures 2F,G). Aside from the lack of unorganized sarcomeres, these data reflect the progressive

nature of HCM phenotypes in the MHC-mutant hiPSC-CMs, as seen in HCM patients.

### 3.4 *MYH7/MYH6* and *MYH7* Mutations Result in Functional Impairment of hiPSC-CMs

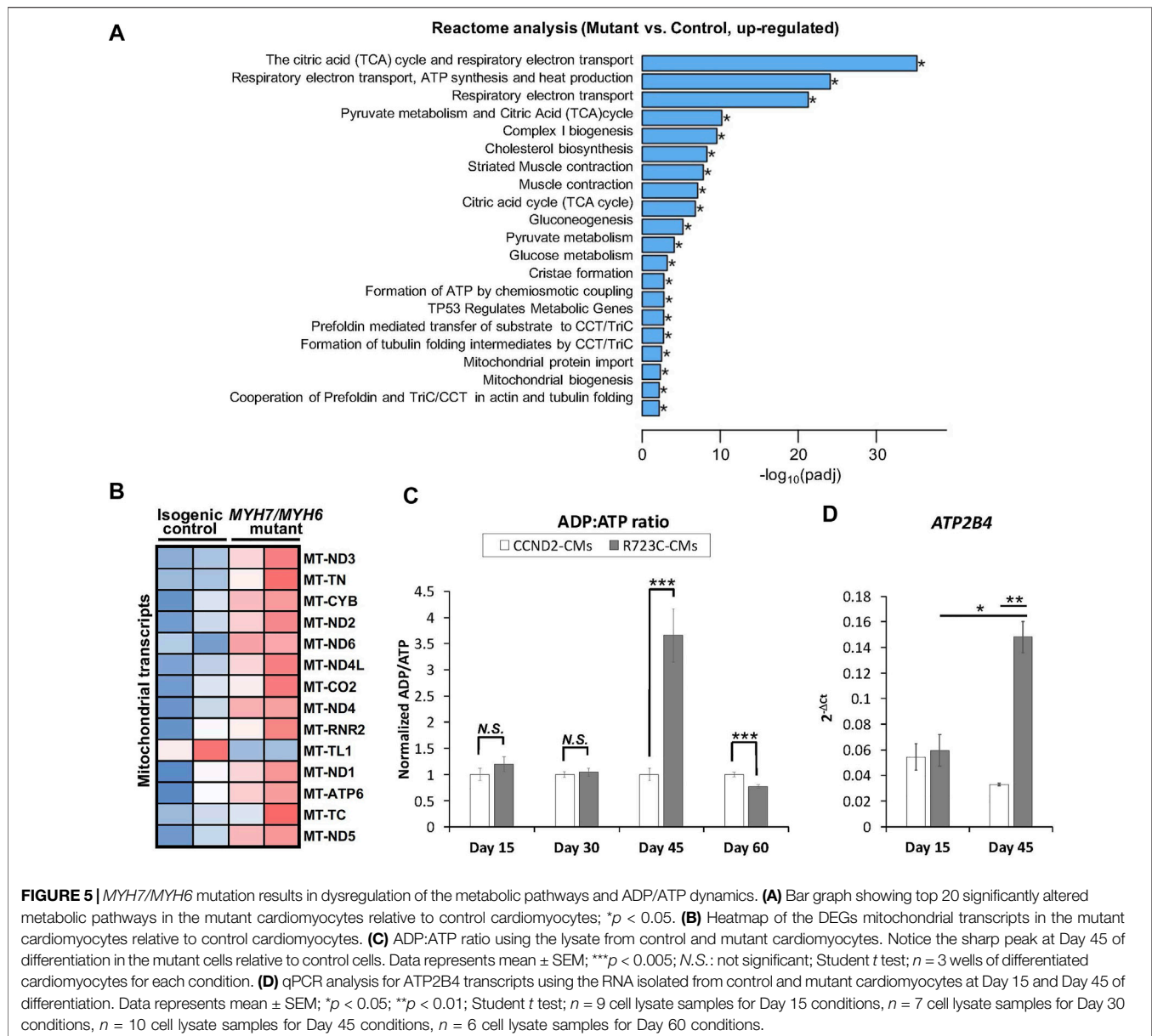
Having established HCM cellular phenotypes, we next studied the impact of *MYH7/MYH6* mutation on cardiomyocyte function. We found that the spontaneous beating rates were





significantly lower in the mutant cardiomyocytes as compared to the control hiPSC-CMs between Day 15–60 of differentiation (Figures 3A,B; Supplementary Video S1). Comparable results of lower spontaneous beat rates were observed in the *MYH7* mutant hiPSC-CMs (Supplementary Figure S3E). The beat rates of the control hiPSC-CMs linearly increased over time, whereas the beat rates of mutant

hiPSC-CMs were not significantly changed between Day 15–45 with a slight decline at Day 60 of differentiation. Further, the maximal spontaneous beat rates of control hiPSC-CMs were significantly higher than the mutant hiPSC-CMs at Day 45 of differentiation (Supplementary Figures 3B,E). Notably, we found statistically more events of irregular beating (arrhythmia) in the mutant hiPSC-CMs at



Day 30 and Day 45 of differentiation (Figures 3A,C,D). We next performed calcium transient measurements using Fluo-4AM fluorescent dye. Our analysis showed a significantly higher calcium signal in the mutant hiPSC-CMs relative to the control hiPSC-CMs at all time points examined (Figure 3E), indicative of increased recruitment of  $\text{Ca}^{2+}$  ions in the mutant cardiomyocytes. Further, similar to the trend of beat rate over time, calcium signal reached maximal value at Day 45 and then declined at Day 60 in the mutant hiPSC-CMs (Figures 3B,E). These results establish the importance of the converter domain of MYH7/MYH6 in the regulation of CM functionality. Also, our result indicates that mutations in the converter domain, such as MYH7 R723C mutation, affects cross-bridge interactions as well as  $\text{Ca}^{2+}$  ion dependency.

### 3.5 Bulk RNAseq Analysis Revealed Alterations in Transcripts Caused by MYH7/MYH6 Mutation

To investigate MYH7/MYH6 mutation-associated molecular details at the early stage of HCM development, we performed bulk RNAseq analysis at Day 15 of differentiation using RNA isolated from the isogenic control and mutant hiPSC-CMs. We performed pair-end sequencing with >30 million reads per sample with clean read counts of more than 96% for each sample (Supplementary Figure S6). Downstream analysis was performed using a combination of programs including STAR, HTseq, Cufflink, and alignments were parsed using Tophat and differential expressions were determined through DESeq2/edgeR R package (3.16.5). The resulting heatmap comparing HCM

mutant and control hiPSC-CMs is shown in **Figure 4A**. From RNA-seq analysis, we identified a total of 3,317 differentially expressed genes (DEGs); of these 49% were upregulated genes and 51% were down-regulated genes in the mutant relative to the control (**Figures 4A–C**). Gene ontology analysis using DisGeNET as well as Disease Ontology (DO) database resources revealed robust enrichment of transcripts involved in hypertrophic cardiomyopathy together with other myopathy-related transcripts (**Figures 4D,E**). Next, our KEGG analysis showed that transcripts up-regulated in the mutant cardiomyocytes were related to hypertrophic cardiomyopathy (*ACTC1*, *MYL2*, *MYL3*),  $\text{Ca}^{2+}$ -dynamics regulatory pathway (*ATP2B4*, *CACNA1C*, *CAMK2B*, *PLN*), as well as cardiac-muscle contraction transcripts (*ACTC1*, *MYH7*, *TNNI3*, *TNNT2*). Given the high degree of the shared homology with *MYH7*, we also included the down-regulated *MYH6* transcript in the cardiac-muscle contraction pathway (**Figures 4F–H**). These studies supported our initial cellular and functional assay in the recapitulation of HCM phenotype in *MYH7/MYH6* mutant cardiomyocytes.

It has been shown that different HCM mutations result in inefficient sarcomeric ATP utilization, energy depletion, and increased ATPase activity of the  $\beta$ -MHC protein (Lan et al., 2013; Mosqueira et al., 2018). To evaluate whether a mutation in the converter domain altered any of these properties, we analyzed the RNAseq datasets for mitochondrial and metabolic pathways. Interestingly, we found robust enrichment of transcripts related to the TCA cycle, respiratory electron-transport pathway, pyruvate metabolism, mitochondrial biogenesis, and complex I biogenesis in the mutant hiPSC-CMs relative to the isogenic control hiPSC-CMs (**Figure 5A**). Additional analysis revealed up-regulation of several mitochondrial transcripts including *MT-ND1-6*, *MT-CYB*, *MT-ATP6* in the mutant hiPSC-CMs (**Figure 5B**). To further support these findings, we performed an ATP/ADP bioluminescence assay using cardiomyocytes from control and mutant lines at various time points. We did not observe any difference in the ADP:ATP ratio until Day 30 of differentiation relative to control hiPSC-CMs. However, we found a robust and sharp increase at Day 45, indicating a surge in the need for ATP utilization at later time points in the mutant hiPSC-CMs as compared to control (**Figure 5C**). Next, we evaluated the expression of *ATP2B4* (an ATPase,  $\text{Ca}^{2+}/\text{Mg}^{2+}$ -dependent enzyme) using RNA isolated from control and mutant lines at Day 15 and Day 45 of differentiation. Similar to ADP:ATP ratio, we found a robust enrichment of *ATP2B4* mRNA at Day 45 of differentiation in the mutant cardiomyocytes relative to control cardiomyocytes (**Figure 5D**). Overall, these data further substantiate the progressive nature of the *MYH7/MYH6* dual mutation-mediated HCM phenotypes.

### 3.6 MYH7/MYH6 Mutation Leads to Changes in ECM Dynamics

Our analysis of the bulk RNAseq datasets revealed several downregulated transcripts in the mutant line including those related to pathways involved in fibrosis, focal adhesion, and

adherent junctions (Varnava et al., 2000). Among several pathways, our Reactome analysis revealed that transcripts related to ECM were most significantly downregulated in the mutant hiPSC-CMs (**Figures 6A,B**), suggesting for the first time that ECM dynamics play a critical role in the development of the HCM phenotype. Our heatmap analysis showed dysregulation of several ECM transcripts such as downregulation of integrin subunits *ITGA2*, *ITGA4*, *ITGA8*, *ITGA9*, *ITGB8*, and up-regulation of *ITGA7*, *ITGAV*, *ITGB1*, *JUN* (**Figure 6B**). Next, our KEGG analysis revealed that genes required for the ECM-receptor interactions were dysregulated in the *MYH7/MYH6* mutant hiPSC-CMs (**Figures 6C,D**). The import of these interactions was further substantiated by the poor adhesion, in terms of cell density and cell spreading, observed in mutant hiPSC-CMs (**Figures 6C,D**; **Supplementary Figure S5D**). Thus, we investigated whether the interaction of the integrins with downstream intracellular signaling pathways and their ability to attach to the Matrigel matrix is altered in the mutant cardiomyocytes. The binding of ECM to integrins induces multiprotein clustering at focal adhesions and mediates intracellular signaling through focal adhesion kinase (FAK) (Guan, 1997). Upon activation, FAK undergoes autophosphorylation (pFAK) and forms a complex with Src and other cellular proteins to trigger downstream signaling through its kinase activity or scaffolding function (Guan, 1997, Guan, 2010). To evaluate this, we performed co-staining using cTnT and pFAK antibodies in the control and mutant hiPSC-CMs. Interestingly, our data revealed activated FAK signaling (pFAK staining), punctate staining near the membrane regions of the control hiPSC-CMs (**Figure 6E**). Notably, this activation was significantly reduced in the mutant hiPSC-CMs with little staining in the membrane regions (**Figure 6E**). Next, to investigate ECM-cell dynamics, among the differentially expressed integrin genes, we selected *ITGB1*, *ITGAV*, and *ITGA2* for flow cytometric analysis to monitor protein level over time. Our data showed up-regulation of *ITGB1* at Day 30 and Day 45 of differentiation and down-regulation of *ITGA2* at Day 30 without a significant change in *ITGAV* levels (**Supplementary Figures S7A–C**). Further, our qPCR analysis revealed higher expression of *ITGAV* and *ITGB1* transcripts using RNA isolated from isogenic control and mutant cardiomyocytes at Day 45 (**Figure 6F**). These studies support the hypothesis that the *MYH7/MYH6* mutation disrupts cell-ECM interactions, leading to a stressed state and perturbed function of cardiomyocytes.

## 4 DISCUSSION

Because HCM is mostly due to sarcomeric protein mutations, novel approaches for investigating HCM genotype-phenotype correlations and molecular mechanisms are essential to identify potential therapeutic targets. In this study, we reviewed the clinical phenotype of the *MYH7* R723C mutation, engineered *MYH7* R723C and *MYH6* R725C mutant hiPSCs using base-editing method, and compared HCM phenotypes in the mutant and corresponding isogenic control hiPSC-CMs. The use of

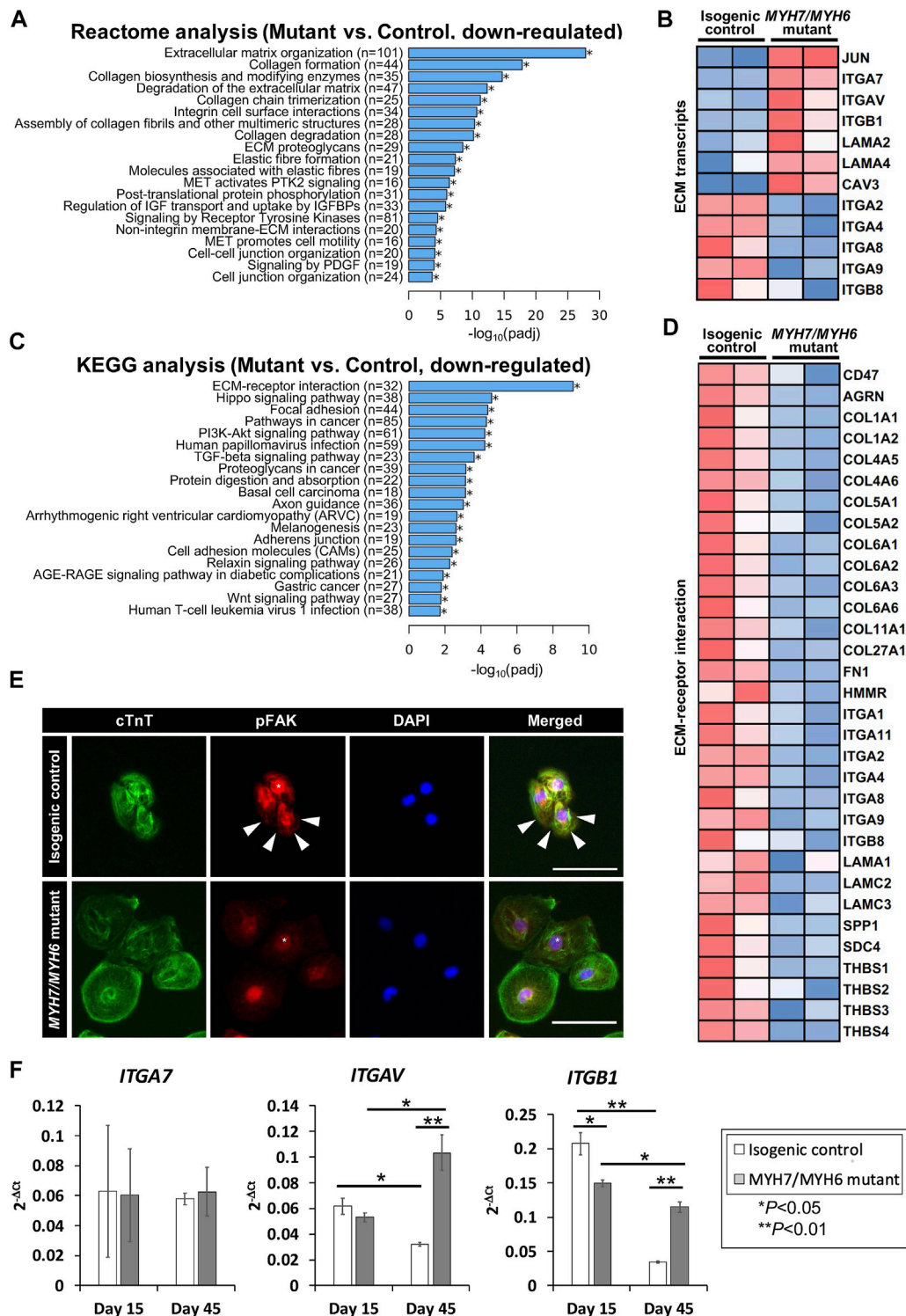


**FIGURE 6 | MYH7/MYH6 mutation drives altered ECM dynamics and ECM-receptor interaction. (A)** Reactome analysis showing the top 20 annotated down-regulated pathways in the mutant as compared to control lines. Note that the most significantly dysregulated were the pathways associated with ECM organization. **(B)** Heatmap showing the dysregulated transcripts involving in ECM. **(C)** Top 20 annotated pathways determined by KEGG analysis with down-regulated DEG list. Note that ECM-receptor interaction transcripts were most significantly altered in the mutant cells relative to control cells. **(D)** Heatmap for up-regulated DEGs that associated with ECM-receptor interaction. **(E)** Representative images of cTnT and pFAK-immunostained hiPSC-CMs using isogenic control and mutant cells. White stars point out nucleus location and white arrows indicate activated FAK signal at the vicinity of the cell-substrate attachment site. DAPI labels the nuclei (blue). (Scale Bar = 100 μm) **(F)** qPCR analysis for *ITGA7*, *ITGAV*, and *ITGB1* transcripts using RNA isolated from control and mutant cardiomyocytes at Day 15 and Day 45 of differentiation. Data represents mean ± SEM; \**p* < 0.05; \*\**p* < 0.01; Student *t* test; *n* = 4 cell lysate samples per condition.

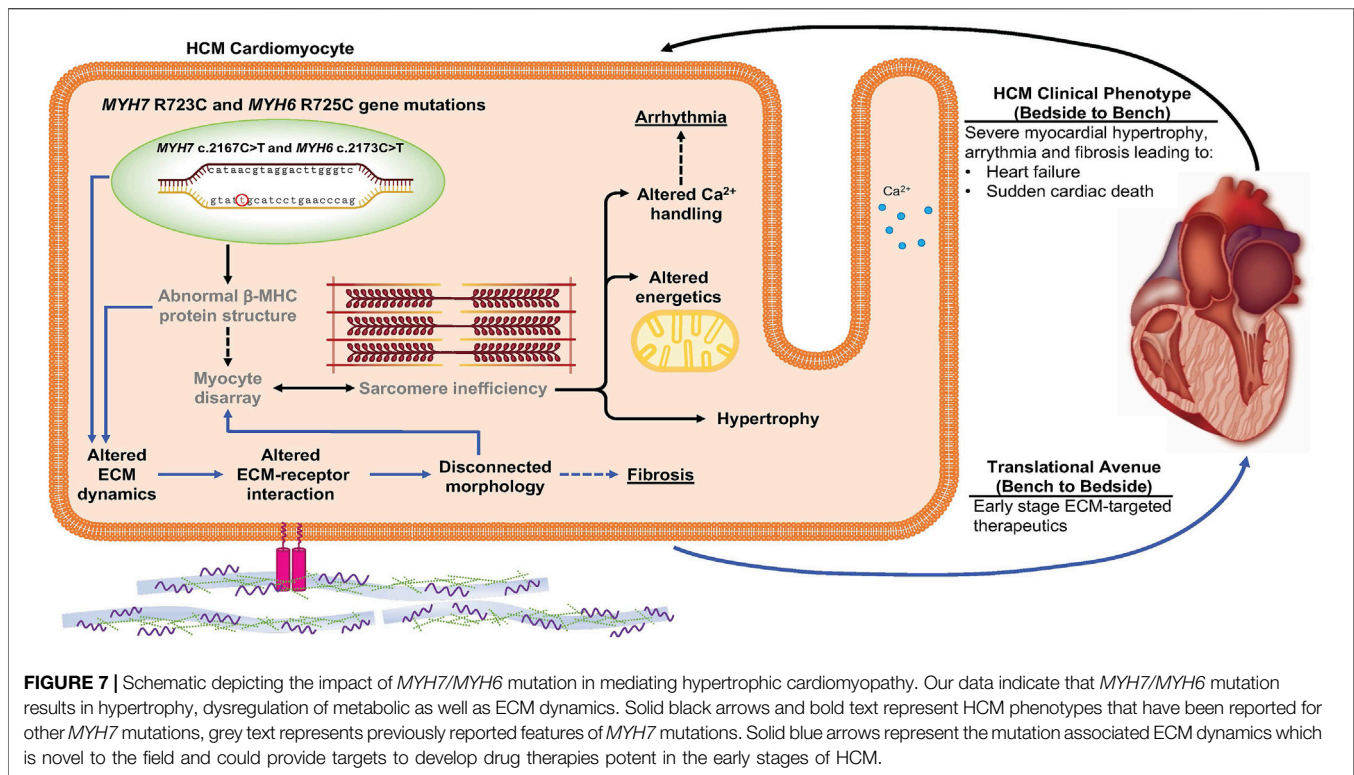


**FIGURE 7 |** Schematic depicting the impact of *MYH7/MYH6* mutation in mediating hypertrophic cardiomyopathy. Our data indicate that *MYH7/MYH6* mutation results in hypertrophy, dysregulation of metabolic as well as ECM dynamics. Solid black arrows and bold text represent HCM phenotypes that have been reported for other *MYH7* mutations, grey text represents previously reported features of *MYH7* mutations. Solid blue arrows represent the mutation associated ECM dynamics which is novel to the field and could provide targets to develop drug therapies potent in the early stages of HCM.

hiPSC-CMs as a model system allowed us to study *early-stage* cell and molecular alterations that give rise to well-described later-stage phenotypes and clinical symptoms of HCM (Sedaghat-Hamedani et al., 2018).

The most significant early-stage molecular alterations detected in *MYH7/MYH6* mutant lines were in ECM remodeling and ECM-receptor interactions. We first noticed that hypertrophy was significant in mutant cells under suspensive condition since Day 15 after the differentiation, while under adherent condition there was no statistically significant difference between the mutant and the control cells at any of the four time points. Since the suspensive cell size only depends on the cell volume and that the adherent cell area would be affected by cell volume as well as cell attachment ability, the discrepancy in cell size obtained from suspensive and adherent conditions suggests defective adhesion of mutant cells. Further, RNAseq, qPCR, and immunostaining data revealed perturbed ECM synthesis and degradation, expression of integrins, and activation of FAK. Integrins are surface receptors and are required for cell-cell interactions as well as cell-matrix interactions (Guan, 1997). Binding of ECM to the integrin receptors is essential for proper intracellular signaling and activation of multi-protein cascades (Guan, 2010). Integrins *ITGAV*, *ITGA7*, and *ITGB1* were upregulated in the mutant hiPSC-CMs, while many ECM genes and others integrins were downregulated. The possibility that these early changes initiate the pathogenesis of the HCM phenotype was further substantiated by the fact that mutant cardiomyocytes became more sparsely dispersed on the plate at later time points perhaps as a function of altered cell-ECM adhesion (**Supplementary Figure S5**). In further support, a study

using *MYH7* R403Q mutation documented the impact of a diseased matrix in prolonged contraction and poor relaxations in engineered heart tissue (EHT) and in a swine model (Sewanani et al., 2019). We depict this new insight regarding early changes in cell-ECM communication as a mediator HCM disease in **Figure 7**. Future studies will be needed to determine whether these outcomes are substantiated in the 3D environment and with mechanical stimulation. We propose drug therapeutics that target these ECM-receptor interactions at the early stages of human development as a new means to prevent or delay the onset of HCM.

We also defined changes in the metabolic pathways and corresponding mitochondrial transcripts in the mutant cardiomyocytes relative to the control. While the observation that metabolic pathways are altered with HCM had been previously reported (Ranjbarvaziri et al., 2021), we add further detail. In particular, we found an aberrant and robust peak in the ADP/ATP dynamics in the mutant hiPSC-CMs at Day 45 of differentiation. However, the defects in beat rate and  $\text{Ca}^{2+}$  amplitude were significantly different starting from Day 15 and plateauing by Day 45. Based on these results, we postulate that in the mutant hiPSC-CMs, there is increased utilization of ATP by the myosin head to continue the next cycles of contraction. These events lead to the accumulation of ADP in the cells, and increased ADP/ATP ratio. We also observed a decline in the ADP/ATP ratio at Day 60 which might be due to a secondary mechanism such as apoptosis or cell loss in the most stressed mutant cardiomyocytes. While these results provide strong evidence for functional defects and ATP utilization in the *MYH7/MYH6* dual mutation-associated HCM, we also

recognize that other factors such as fiber stiffness (Kohler et al., 2002) and contraction velocity (Kawana et al., 2017) might also contribute to this phenotype and will be the focus of future studies.

We also provide evidence for increased mitochondrial load and changes in metabolic profiling in the mutant hiPSC-CMs. Whether this is due to the *MYH7/MYH6* mutations in the converter domain of MHC with increased fiber stiffness, the requirement of higher energy, or imperfect interactions of actin-myosin bridging is not clear from this study. Further biochemical assays will be needed to answer these questions. It has been shown that other *MYH7* mutations, R723G as well as R719W, resulted in a 15% increase in gliding velocities (Kawana et al., 2017). Similarly, among individual cardiomyocytes, R723G showed heterogeneity in cell-cell interaction and force generation, presumably due to differential levels of myosin proteins in each cell (Kraft et al., 2016). Surprisingly, we identified a cascade of fibrotic transcripts to be down-regulated in the mutant cardiomyocytes. Since fibrosis and myocyte disarray are hallmark features of HCM (Varnava et al., 2000; Maron and Maron, 2013), we believe that the downregulation of fibrotic pathways could be a compensatory mechanism to reduce the functional load on the mutant cardiomyocytes.

It should be noted that genetic testing for patients with an HCM phenotype is recommended in the current guidelines and assesses 8 sarcomeric genes with strong evidence to be disease causing in HCM, including *MYH7* (Ommen et al., 2020). Genetic testing can be utilized for screening family members who may be at risk for developing HCM, however mutation type is not currently able to predict the risk of SCD or guide clinical management. However, genetic testing can be clinically important in those patients with greater than 1 sarcomeric gene mutation and HCM phenotype, as they may have more severe disease (Kelly and Semsarian, 2009; Girolami et al., 2010; Maron et al., 2012; Weissler-Snir et al., 2017; Riaz et al., 2022). Girolami et al. described a HCM patient with *MYH7* R723C, E1455X, and *MYBPC3* E165D who underwent cardiac transplantation at the age of 43. Recently, Riaz et al. described a *MYH7* R723C and *MLP* W4R dual mutation in a 1-year-old patient with severe obstructive asymmetric hypertrophy necessitating septal myectomy. In these patients with dual *MYH7* R723C mutations, they have had early pathogenic phenotypes. Therefore, dual and triple mutations in *MYH7* and other sarcomeric genes in patients have demonstrated a more severe disease course in patients with HCM. However, there are no animal models nor hiPSC models of dual or triple HCM mutations. Prior studies using hiPSC-CMs have focused on single sarcomeric HCM mutations (Lan et al., 2013; Han et al., 2014). Here we have evaluated the impact of two sarcomeric mutations in hiPSC-CM, including a known pathogenic mutation (*MYH7* R723C) and a variant of unknown significance (*MYH6* R725C). We have assessed the molecular and physiologic impact of the double and single pathogenic mutations at an early-stage including calcium dysregulation, cellular hypertrophy, altered energetics, and altered extracellular matrix dynamics. While *MYH6* mutations have been described to result in HCM, they are not routinely tested in

the sarcomeric gene panel. Patients with other sarcomeric gene mutations may have other relevant HCM causing gene mutations that are not being captured with routine genetic testing. Our study provides evidence of later-stage HCM phenotype with dual mutations and suggests developing a broader panel of mutations or whole genome sequencing to screen individuals with a genetic propensity for HCM or with advanced symptoms may improve the ability of genetic testing to guide treatment and/or predict disease penetrance.

Because hiPSC-CMs are relatively immature when cultured in 2D without exogenous stimulation, they uniquely facilitate the understanding of early-stage, direct consequences of HCM mutation(s) without other secondary changes in animal models or patients. Based on single-cell 2D cardiac differentiation showing that *MYH6* is abundant at day 12 and subsequently *MYH7* predominates (Grancharova et al., 2021), we assessed an early time point (Day 15) and a later time point (Day 45) to facilitate the early-stage understanding of the functional contributions of *MYH6* as well as *MYH7* converter domain mutations. Additionally, generation of hiPSCs with multiple HCM mutations including variants of unknown significance or sarcomere gene negative HCM, may allow understanding of early stage molecular and physiologic changes that have been challenging to assess in animal models or patients. Further, modeling double or multiple HCM mutations in hiPSC-CMs may elucidate the interaction between multiple sarcomeric proteins.

In summary, our data demonstrated that HCM phenotypes can be recapitulated using hiPSC-CMs with *MYH7* R723C and *MYH6* R725C mutations, and that changes in gene expression at early stages of differentiation could offer clues for novel therapeutic classes to prevent or delay the onset of HCM cellular and functional phenotypes. Future work to generate *MYH7* R723C mutant models in a 3D environment, like the human chambered muscle pump (hChAMP) (Kupfer et al., 2020) or engineered heart tissue (Yang et al., 2018), with supportive cells, such as fibroblasts, will help to further elucidate the role of the ECM in driving the phenotypic characteristics of HCM.

## DATA AVAILABILITY STATEMENT

The original contributions presented in the study are publicly available. The transcriptomic data can be found here: <https://www.ncbi.nlm.nih.gov/sra/GSE198258>.

## AUTHOR CONTRIBUTIONS

JH, KB, EK, BW, BS, and BO conceived and designed the research. KB, BM, and BW generated the R723C mutant hiPSCs. JH designed and executed the experiments including cardiac differentiation, functional measurements, endpoint sample collection, immunostaining, imaging, and quantitative analysis, RNAseq analysis, and flow cytometry analysis. BS performed qPCR analysis, ATP/ADP assay, pFAK

staining and interpreted RNAseq result. FK helped with the clinical data analysis and summarized the clinical outcomes. SG analyzed blinded data for multinucleation and sarcomeric organization. JL helped interpret RNAseq result. JH, FK, BS, and BO discussed the results, wrote and edited the manuscript. All authors approved the manuscript.

## FUNDING

This research was supported by Regenerative Medicine Minnesota (RMM 091620DS008 to BO and BS), the American Heart Association (#21Predoc836194 to JH) and the National Heart, Lung, and Blood Institute of the National Institutes of Health (R01 HL137204 to BO).

## REFERENCES

- Alpert, N. R., Brosseau, C., Federico, A., Krenz, M., Robbins, J., and Warshaw, D. M. (2002). Molecular Mechanics of Mouse Cardiac Myosin Isoforms. *Am. J. Physiol.-Heart Circul. Physiol.* 283, H1446–H1454. doi:10.1152/ajpheart.00274.2002
- Becker, K. D., Gottshall, K. R., Hickey, R., Perriard, J.-C., and Chien, K. R. (1997). Point Mutations in Human Beta Cardiac Myosin Heavy Chain Have Differential Effects on Sarcomeric Structure and Assembly: an ATP Binding Site Change Disrupts Both Thick and Thin Filaments, whereas Hypertrophic Cardiomyopathy Mutations Display Normal Assembly. *J. Cell Biol.* 137, 131–140. doi:10.1083/jcb.137.1.131
- Bhagwan, J. R., Mosqueira, D., Chairez-Cantu, K., Mannhardt, I., Bodbin, S. E., Bakar, M., et al. (2020). Isogenic Models of Hypertrophic Cardiomyopathy Unveil Differential Phenotypes and Mechanism-Driven Therapeutics. *J. Mol. Cell. Cardiol.* 145, 43–53. doi:10.1016/j.yjmcc.2020.06.003
- Bjornsson, T., Thorolfsson, R. B., Sveinbjornsson, G., Sulem, P., Norddahl, G. L., Helgadóttir, A., et al. (2018). A Rare Missense Mutation in MYH6 Associates with Non-syndromic Coarctation of the Aorta. *Eur. heart J.* 39 (34), 3243–3249. doi:10.1093/eurheartj/ehy142
- Burke, M. A., Cook, S. A., Seidman, J. G., and Seidman, C. E. (2016). Clinical and Mechanistic Insights into the Genetics of Cardiomyopathy. *J. Am. Coll. Cardiol.* 68, 2871–2886. doi:10.1016/j.jacc.2016.08.079
- Gaudelli, N. M., Komor, A. C., Rees, H. A., Packer, M. S., Badran, A. H., Bryson, D. I., et al. (2017). Programmable Base Editing of A\*T to G\*C in Genomic DNA without DNA Cleavage. *Nature* 551, 464–471. doi:10.1038/nature24644
- Girolami, F., Ho, C. Y., Semsarian, C., Baldi, M., Will, M. L., Baldini, K., et al. (2010). Clinical Features and Outcome of Hypertrophic Cardiomyopathy Associated with Triple Sarcomere Protein Gene Mutations. *J. Am. Coll. Cardiol.* 55, 1444–1453. doi:10.1016/j.jacc.2009.11.062
- Grancharova, T., Gerbin, K. A., Rosenberg, A. B., Roco, C. M., Arakaki, J. E., DeLizo, C. M., et al. (2021). A Comprehensive Analysis of Gene Expression Changes in a High Replicate and Open-Source Dataset of Differentiating hiPSC-Derived Cardiomyocytes. *Sci. Rep.* 11, 15845. doi:10.1038/s41598-021-94732-1
- Guan, J.-L. (1997). Role of Focal Adhesion Kinase in Integrin Signaling. *Int. J. Biochem. Cell Biol.* 29, 1085–1096. doi:10.1016/s1357-2725(97)00051-4
- Guan, J.-L. (2010). Integrin Signaling through FAK in the Regulation of Mammary Stem Cells and Breast Cancer. *IUBMB Life* 62, 268–76. doi:10.1002/iub.303
- Han, L., Li, Y., Tchoa, J., Kaplan, A. D., Lin, B., Li, Y., et al. (2014). Study Familial Hypertrophic Cardiomyopathy Using Patient-specific Induced Pluripotent Stem Cells. *Cardiovasc Res.* 104, 258–269. doi:10.1093/cvr/cvu205
- Holm, H., Gudbjartsson, D. F., Sulem, P., Masson, G., Helgadóttir, H. T., Zanon, C., et al. (2011). A Rare Variant in MYH6 is Associated With High Risk of Sick Sinus Syndrome. *Nat. Genet.* 43 (4), 316–320. doi:10.1038/ng.781

## ACKNOWLEDGMENTS

We acknowledge the help from Wei-Han Lin for carrying out the contractility and calcium assays. We acknowledge Dr. Ryan Knoper for helpful discussion about the clinical manifestation and characteristics of hypertrophic cardiomyopathy.

## SUPPLEMENTARY MATERIAL

The Supplementary Material for this article can be found online at: <https://www.frontiersin.org/articles/10.3389/fcell.2022.894635/full#supplementary-material>

**Supplementary Video S1** | This video shows a side-by-side comparison of morphology and beat profile in MYH7/MYH6 mutant hiPSC-CMs and isogenic control hiPSC-CMs.

- Homburger, J. R., Green, E. M., Caleshu, C., Sunitha, M. S., Taylor, R. E., Ruppel, K. M., et al. (2016). Multidimensional Structure-Function Relationships in Human Beta-Cardiac Myosin from Population-Scale Genetic Variation. *Proc. Natl. Acad. Sci. U.S.A.* 113, 6701–6706. doi:10.1073/pnas.1606950113
- Kawana, M., Sarkar, S. S., Sutton, S., Ruppel, K. M., and Spudich, J. A. (2017). Biophysical Properties of Human Beta-Cardiac Myosin with Converter Mutations that Cause Hypertrophic Cardiomyopathy. *Sci. Adv.* 3, e1601959. doi:10.1126/sciadv.1601959
- Kelly, M., and Semsarian, C. (2009). Multiple Mutations in Genetic Cardiovascular Disease: a Marker of Disease Severity? *Circ. Cardiovasc. Genet.* 2, 182–190. doi:10.1161/CIRCGENETICS.108.836478
- Köhler, J., Winkler, G., Schulte, I., Scholz, T., McKenna, W., Brenner, B., et al. (2002). Mutation of the Myosin Converter Domain Alters Cross-Bridge Elasticity. *Proc. Natl. Acad. Sci. U.S.A.* 99, 3557–3562. doi:10.1073/pnas.062415899
- Kraft, T., Montag, J., Radocaj, A., and Brenner, B. (2016). Hypertrophic Cardiomyopathy: Cell-To-Cell Imbalance in Gene Expression and Contraction Force as Trigger for Disease Phenotype Development. *Circ. Res.* 119, 992–995. doi:10.1161/CIRCRESAHA.116.309804
- Kupfer, M. E., Lin, W.-H., Ravikumar, V., Qiu, K., Wang, L., Gao, L., et al. (2020). *In Situ* Expansion, Differentiation, and Electromechanical Coupling of Human Cardiac Muscle in a 3D Bioprinted, Chambered Organoid. *Circ. Res.* 127, 207–224. doi:10.1161/CIRCRESAHA.119.316155
- Lan, F., Lee, A. S., Liang, P., Sanchez-Freire, V., Nguyen, P. K., Wang, L., et al. (2013). Abnormal Calcium Handling Properties Underlie Familial Hypertrophic Cardiomyopathy Pathology in Patient-specific Induced Pluripotent Stem Cells. *Cell Stem Cell* 12, 101–113. doi:10.1016/j.stem.2012.10.010
- Lian, X., Hsiao, C., Wilson, G., Zhu, K., Hazeltine, L. B., Azarin, S. M., et al. (2012). Robust Cardiomyocyte Differentiation from Human Pluripotent Stem Cells via Temporal Modulation of Canonical Wnt Signaling. *Proc. Natl. Acad. Sci. U.S.A.* 109, E1848–E1857. doi:10.1073/pnas.1200250109
- Locher, M. R., Razumova, M. V., Stelzer, J. E., Norman, H. S., Patel, J. R., and Moss, R. L. (2009). Determination of Rate Constants for Turnover of Myosin Isoforms in Rat Myocardium: Implications for *In Vivo* Contractile Kinetics. *Am. J. Physiol.-Heart Circul. Physiol.* 297, H247–H256. doi:10.1152/ajpheart.00922.2008
- Lowes, B. D., Minobe, W., Abraham, W. T., Rizeq, M. N., Bohlmeier, T. J., Quafe, R. A., et al. (1997). Changes in Gene Expression in the Intact Human Heart. Downregulation of Alpha-Myosin Heavy Chain in Hypertrophied, Failing Ventricular Myocardium. *J. Clin. Invest.* 100, 2315–2324. doi:10.1172/JCI119770
- Lowey, S., Lesko, L. M., Rovner, A. S., Hodges, A. R., White, S. L., Low, R. B., et al. (2008). Functional Effects of the Hypertrophic Cardiomyopathy R403Q Mutation Are Different in an Alpha- or Beta-Myosin Heavy Chain Backbone. *J. Biol. Chem.* 283, 20579–20589. doi:10.1074/jbc.M800554200

- Kluesner, M. G., Nedveck, D. A., Lahr, W. S., Garbe, J. R., Abrahante, J. E., Webber, B. R., and Moriarity, B. S. (2018). EditR: A Method to Quantify Base Editing from Sanger Sequencing. *The CRISPR journal*, 1(3), 239–250. doi:10.1089/crispr.2018.0014
- Komor, A. C., Kim, Y. B., Packer, M. S., Zuris, J. A., and Liu, D. R. (2016). Programmable editing of a target base in genomic DNA without double-stranded DNA cleavage. *Nature*, 533(7603), 420–424. doi:10.1038/nature17946
- Marian, A. J., and Braunwald, E. (2017). Hypertrophic Cardiomyopathy: Genetics, Pathogenesis, Clinical Manifestations, Diagnosis, and Therapy. *Circ. Res.* 121, 749–770. doi:10.1161/CIRCRESAHA.117.311059
- Maron, B. J., and Maron, M. S. (2013). Hypertrophic Cardiomyopathy. *Lancet* 381, 242–255. doi:10.1016/S0140-6736(12)60397-3
- Maron, B. J., Maron, M. S., and Semsarian, C. (2012). Double or Compound Sarcomere Mutations in Hypertrophic Cardiomyopathy: a Potential Link to Sudden Death in the Absence of Conventional Risk Factors. *Heart Rhythm*. 9, 57–63. doi:10.1016/j.hrthm.2011.08.009
- McNally, E. M., Gianola, K. M., and Leinwand, L. A. (1989). Complete Nucleotide Sequence of Full Length cDNA for Rat  $\alpha$  Cardiac Myosin Hea Chain. *Nucl. Acids Res.* 17, 7527–7528. doi:10.1093/nar/17.18.7527
- Mosqueira, D., Mannhardt, I., Bhagwan, J. R., Lis-Slimak, K., Katili, P., Scott, E., et al. (2018). CRISPR/Cas9 Editing in Human Pluripotent Stem Cell-Cardiomyocytes Highlights Arrhythmias, Hypocontractility, and Energy Depletion as Potential Therapeutic Targets for Hypertrophic Cardiomyopathy. *Eur. Heart J.* 39, 3879–3892. doi:10.1093/eurheartj/ehy249
- Niimura, H., Patton, K. K., McKenna, W. J., Soultis, J., Maron, B. J., Seidman, J. G., et al. (2002). Sarcomere Protein Gene Mutations in Hypertrophic Cardiomyopathy of the Elderly. *Circulation* 105 (4), 446–451. doi:10.1161/hc0402.102990
- Ommen, S. R., Mital, S., Burke, M. A., Day, S. M., Deswal, A., Elliott, P., et al. (2020). 2020 AHA/ACC Guideline for the Diagnosis and Treatment of Patients with Hypertrophic Cardiomyopathy: A Report of the American College of Cardiology/American Heart Association Joint Committee on Clinical Practice Guidelines. *J. Am. Coll. Cardiol.* 76, e159–e240. doi:10.1016/j.jacc.2020.08.045
- Ranjbarvaziri, S., Kooiker, K. B., Ellenberger, M., Fajardo, G., Zhao, M., Vander Roest, A. S., et al. (2021). Altered Cardiac Energetics and Mitochondrial Dysfunction in Hypertrophic Cardiomyopathy. *Circulation* 144 (21), 1714–1731. doi:10.1161/CIRCULATIONAHA.121.053575
- Riaz, M., Park, J., Sewanan, L. R., Ren, Y., Schwan, J., Das, S. K., et al. (2022). Muscle LIM Protein Force-Sensing Mediates Sarcomeric Biomechanical Signaling in Human Familial Hypertrophic Cardiomyopathy. *Circulation* 145 (16), 1238–1253. doi:10.1161/CIRCULATIONAHA.121.056265
- Rose, J., Kraft, T., Brenner, B., and Montag, J. (2020). Hypertrophic Cardiomyopathy MYH7 Mutation R723G Alters mRNA Secondary Structure. *Physiol. Genomics* 52, 15–19. doi:10.1152/physiolgenomics.00100.2019
- Sedaghat-Hamedani, F., Kayvanpour, E., Tugrul, O. F., Lai, A., Amr, A., Haas, J., et al. (2018). Clinical Outcomes Associated with Sarcomere Mutations in Hypertrophic Cardiomyopathy: a Meta-Analysis on 7675 Individuals. *Clin. Res. Cardiol.* 107, 30–41. doi:10.1007/s00392-017-1155-5
- Semsarian, C., Ingles, J., Maron, M. S., and Maron, B. J. (2015). New Perspectives on the Prevalence of Hypertrophic Cardiomyopathy. *J. Am. Coll. Cardiol.* 65, 1249–1254. doi:10.1016/j.jacc.2015.01.019
- Sewanan, L. R., Schwan, J., Kluger, J., Park, J., Jacoby, D. L., Qyang, Y., et al. (2019). Extracellular Matrix from Hypertrophic Myocardium Provokes Impaired Twitch Dynamics in Healthy Cardiomyocytes. *JACC Basic Transl. Sci.* 4, 495–505. doi:10.1016/j.jacbs.2019.03.004
- Toepfer, C. N., Garfinkel, A. C., Venturini, G., Wakimoto, H., Repetti, G., Alamo, L., et al. (2020). Myosin Sequestration Regulates Sarcomere Function, Cardiomyocyte Energetics, and Metabolism, Informing the Pathogenesis of Hypertrophic Cardiomyopathy. *Circulation* 141 (10), 828–842. doi:10.1161/CIRCULATIONAHA.119.042339
- Vander Roest, A. S., Liu, C., Morck, M. M., Kooiker, K. B., Jung, G., Song, D., et al. (2021). Hypertrophic Cardiomyopathy  $\beta$ -cardiac Myosin Mutation (P710R) Leads to Hypercontractility by Disrupting Super Relaxed State. *Proc. Natl. Acad. Sci. U.S.A.* 118 (24), e2025030118. doi:10.1073/pnas.2025030118
- Varnava, A. M., Elliott, P. M., Sharma, S., McKenna, W. J., and Davies, M. J. (2000). Hypertrophic Cardiomyopathy: the Interrelation of Disarray, Fibrosis, and Small Vessel Disease. *Heart* 84, 476–482. doi:10.1136/heart.84.5.476
- Webber, B. R., Lonetree, C.-I., Kluesner, M. G., Johnson, M. J., Pomeroy, E. J., Diers, M. D., et al. (2019). Highly Efficient Multiplex Human T Cell Engineering without Double-Strand Breaks Using Cas9 Base Editors. *Nat. Commun.* 10, 5222. doi:10.1038/s41467-019-13007-6
- Weissler-Snir, A., Adler, A., Williams, L., Gruner, C., and Rakowski, H. (2017). Prevention of Sudden Death in Hypertrophic Cardiomyopathy: Bridging the Gaps in Knowledge. *Eur. Heart J.* 38, ehv268–1737. doi:10.1093/eurheartj/ehv268
- Yang, K.-C., Breitbart, A., De Lange, W. J., Hofsteen, P., Futakuchi-Tsuchida, A., Xu, J., et al. (2018). Novel Adult-Onset Systolic Cardiomyopathy Due to MYH7 E848G Mutation in Patient-Derived Induced Pluripotent Stem Cells. *JACC Basic Transl. Sci.* 3, 728–740. doi:10.1016/j.jacbs.2018.08.008
- Zhao, M., Nakada, Y., Wei, Y., Bian, W., Chu, Y., Borovjagin, A. V., et al. (2021). Cyclin D2 Overexpression Enhances the Efficacy of Human Induced Pluripotent Stem Cell-Derived Cardiomyocytes for Myocardial Repair in a Swine Model of Myocardial Infarction. *Circulation* 144 (3), 210–228. doi:10.1161/CIRCULATIONAHA.120.049497
- Zhu, W., Zhao, M., Mattapally, S., Chen, S., and Zhang, J. (2018). CCND2 Overexpression Enhances the Regenerative Potency of Human Induced Pluripotent Stem Cell-Derived Cardiomyocytes: Remuscularization of Injured Ventricle. *Circ. Res.* 122 (1), 88–96. doi:10.1161/CIRCRESAHA.117.311504

**Conflict of Interest:** The authors declare that the research was conducted in the absence of any commercial or financial relationships that could be construed as a potential conflict of interest.

**Publisher's Note:** All claims expressed in this article are solely those of the authors and do not necessarily represent those of their affiliated organizations, or those of the publisher, the editors and the reviewers. Any product that may be evaluated in this article, or claim that may be made by its manufacturer, is not guaranteed or endorsed by the publisher.

Copyright © 2022 Hsieh, Becklin, Givens, Komosa, Lloréns, Kamdar, Moriarity, Webber, Singh and Ogle. This is an open-access article distributed under the terms of the Creative Commons Attribution License (CC BY). The use, distribution or reproduction in other forums is permitted, provided the original author(s) and the copyright owner(s) are credited and that the original publication in this journal is cited, in accordance with accepted academic practice. No use, distribution or reproduction is permitted which does not comply with these terms.